PAPER

Moments of the inverse participation ratio for the Laplacian on finite regular graphs

View the article online for updates and enhancements.

IOP ebooks™

Bringing you innovative digital publishing with leading voices to create your essential collection of books in STEM research.

Start exploring the collection - download the first chapter of every title for free.

Moments of the inverse participation ratio for the Laplacian on finite regular graphs

Timothy B P Clark[1] and Adrian Del Maestro[2]

[1] Department of Mathematics and Statistics, Loyola University Maryland, Baltimore, MD 21211, United States of America
[2] Department of Physics, University of Vermont, Burlington, VT 05405, United States of America

E-mail: tbclark@loyola.edu and Adrian.DelMaestro@uvm.edu

CrossMark

Abstract

We investigate the first and second moments of the inverse participation ratio (IPR) for all eigenvectors of the Laplacian on finite random regular graphs with n vertices and degree z. By exactly diagonalizing a large set of z-regular graphs, we find that as n becomes large, the mean of the inverse participation ratio on each graph, when averaged over a large ensemble of graphs, approaches the numerical value 3. This universal number is understood as the large-n limit of the average of the quartic polynomial corresponding to the IPR over an appropriate $(n-2)$-dimensional hypersphere of $\mathbb{R}^n$. For a large, but not exhaustive ensemble of graphs, the mean variance of the inverse participation ratio for all graph Laplacian eigenvectors deviates from its continuous hypersphere average due to large graph-to-graph fluctuations that arise from the existence of highly localized modes.

(Some figures may appear in colour only in the online journal)

1. Introduction

Much of condensed matter physics involves the study of either localized or itinerant degrees of freedom that exist on the sites of a Euclidean lattice, defined by a notion of physical distance between a site and some number of proximate or 'neighboring' ones. The relationship between a site and its neighbors defines both the dimension of space, d and a finite set of lattice vectors $a_j \in \mathbb{R}^d$, $j = 1, \ldots, d$ that can be used in combination with a set of integers $\{\boldsymbol{m}\}$ with $\boldsymbol{m}_i \in \mathbb{Z}^d$ to index n lattice sites via $\boldsymbol{R}_i = \sum_{j=1}^d m_{ij} a_j$. Examples include the fourteen

Bravais lattices in three spatial dimensions. However, it is often instructive to consider the same physical degrees of freedom on a non-Euclidean lattice, or graph, where no distance metric exists. A finite lattice of n sites is replaced by a graph G, consisting of a set of vertices $V = \{v_i\}$, each connected by z_i undirected edges to its neighboring vertices. The quantity z_i is known as the *degree* of the vertex v_i, and is equivalent to twice the spatial dimension for a hypercubic lattice.

Studying a given physical model on a graph offers many technical benefits including the ability to: (i) study arbitrarily long range interactions where exact mean-field solutions may be available, (ii) smoothly tune and control the local dimensionality and (iii) easily encode the randomness and disorder that often exists in real systems. Celebrated examples from statistical physics include the solution of the Ising model and its generalizations; graph coloring and random percolation problems (for a review see [1]). Anderson's model of non-interacting electrons hopping on a disordered lattice [2] was first solved on the Cayley tree (Bethe lattice) [3], providing deep physical insights into the nature of localization in quantum mechanical systems. More recently, the ability to study graphs in the limit $z \to \infty$ has lead to the development of dynamical mean field theory [4], allowing for systematic investigations of candidate microscopic models of the high temperature superconductors [5].

The discrete Laplacian matrix L plays a crucial role in defining any physical model on a graph, as it quantifies the energy cost of rapidly varying some local degree of freedom among a set of neighboring vertices. For example, it encodes the classical dynamics in random vibrational networks [6] as well the onset of ferromagnetism in the classical [7] and quantum $O(n)$ model [8, 9] on graphs. It appears in models of non-interacting bosons hopping between graph vertices, where the existence of a Bose–Einstein condensation transition on complex networks can be rigorously proven [10].

In this paper, we are interested in the properties of the Laplacian defined on finite sized *regular* graphs, defined by the constraint that each of the n vertices is connected to exactly z neighbors. Examples with $n = 100$ and $z = 3, 8$ are shown in figure 1. Such graphs possess many important mathematical properties [14] while still retaining similarities to the physically realizable Bravais lattices discussed above.

Much is known about the spectral properties of random regular graphs, both in the thermodynamic limit $n \to \infty$ [15–17] and more recently, at finite (but large) n [18–21]. The analyses of spectral statistics have yielded fruitful and universal connections [22] between random regular graphs and the Gaussian orthogonal ensemble of random matrix theory [23–25] known to be relevant in describing the fluctuations of energy levels in physical dynamical systems.

Substantially less is known about the eigenvectors of L [26] with early work focusing on empirical analyses of nodal domains [27, 28] or specific vectors [29], as it is not possible to apply many of the standard tools of analysis for Euclidean lattices, including the Fourier transform. Subsequently, a series of results [18, 21, 30, 31] have shown that for suitably large n, the eigenvectors of random regular graphs are delocalized—they have few non-zero entries. Very recently, the breakthrough works of Bourgade *et al* [32] and Backhausz and Szegedy [33] have proven exiting new results that the eigenvector components are Gaussian independent and identically distributed for large n. To our knowledge, the physical implications of these new results for finite realizations of z and n amenable to direct numerical analysis have yet to be explored.

To address this gap, we systematically study the eigenvectors of the Laplacian matrix on a large class of finite size random regular graphs through brute-force numerical diagonalization. We investigate the statistics of the inverse participation ratio, a scalar proxy for localization, and numerically observe that its mean across all eigenvectors approaches a finite universal
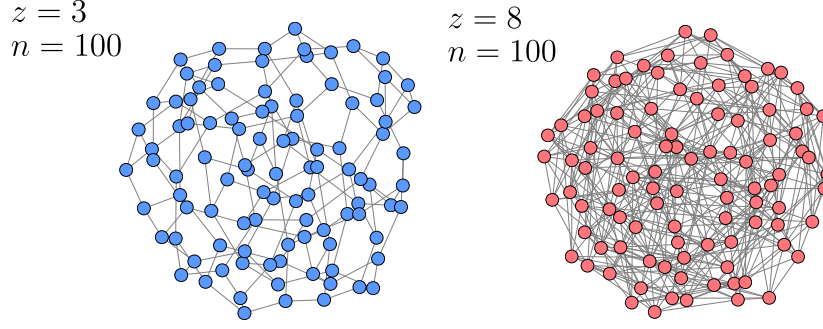
Figure 1. Regular graphs with $n = 100$ vertices and degrees $z = 3$ and $z = 8$ constructed using `NetworkX` [11] via the Steger–Wormald algorithm [12, 13].

value equal to 3, independent of graph degree. We quantify the second moment of the distribution and find a dependence both on degree z and the number of vertices n.

The paper is organized as follows: we begin with a formal definition of the discrete Laplacian on graphs in sections 2 and describe our numerical results for the inverse participation ratio in section 3. In section 4, we analyze the inverse participation ratio as a polynomial function on an $(n-2)$-dimensional subsphere of n-dimensional real space. This perspective allows us to calculate exact values for the first and second moments of the inverse participation ratio over a continuous domain which contains the (terminal points of the) eigenvectors of the Laplacian. Section 5 compares the values of the theoretically derived moments to those numerically computed from a large set of finite size random regular graphs. We analyze the deviations from the theoretically derived second moment with a discussion of localized eigenvectors and highlight implications for their use in computing physical observables on finite random regular graphs.

2. The graph Laplacian

The Laplacian matrix generalizes the continuous Laplace operator $\Delta \equiv \boldsymbol{\nabla} \cdot \boldsymbol{\nabla}$ to encode variations of any continuous function $\phi : V \to \mathbb{C}$ which can take a value ϕ_i on the vertex v_i. The physical importance of this matrix stems from the fact that solutions of $\Delta \phi = 0$ correspond to the Dirichlet energy functional which is stationary in some spatial region. The particular extension of Δ to a graph that we employ arises from the discrete approximation to the second continuous derivative of ϕ on a hypercubic lattice in d spatial dimensions with unit lattice spacing:

$$\Delta \phi(\boldsymbol{R}_i) \approx \sum_{j=1}^{d} \left[\phi\left(\boldsymbol{R}_i + \boldsymbol{e}_j\right) + \phi\left(\boldsymbol{R}_i - \boldsymbol{e}_j\right) - 2\phi\left(\boldsymbol{R}_i\right) \right] \tag{1}$$

where $\boldsymbol{e}_j$ are the Cartesian unit vectors with elements $e_{kj} = \delta_{kj}$ and δ_{kj} is the Kronecker δ-function. On a regular graph G consisting of n vertices v_i, each with degree z, the local connectivity is encoded in an adjacency matrix A_{ij} where

$$A_{ij} = \begin{cases} 1; & \text{if } v_i \text{ and } v_j \text{ share an edge,} \\ 0; & \text{otherwise.} \end{cases} \tag{2}$$

Comparing with equation (1), we can write the elements of the graph Laplacian matrix as the difference between the degree and adjacency matrices of G:

$$L_{ij} = z\delta_{ij} - A_{ij} \tag{3}$$

and observe that z corresponds to twice the dimension on a hypercubic lattice. As mentioned in the introduction, L may appear in the Hamiltonian of numerous physical systems defined on a graph in the form:

$$H = \frac{1}{2} \sum_{i,j=1}^{n} \phi_i^* L_{ij} \phi_j . \tag{4}$$

A spectral decomposition of L provides a route to the determination of the equations of motion governing a classical system, or the nature of the wavefunctions and allowed energy eigenstates for a quantum mechanical one.

2.1. Exact diagonalization

We now focus on the spectral decomposition of Laplacian matrices drawn from an ensemble of random regular graphs with with n vertices and degree z. These matrices are generated using the $O(nz^2)$ algorithm of Steger and Wormald [12]. From the vertex neighbor list of each graph, we construct the adjacency matrix A and then exactly diagonalize the resulting $n \times n$ sparse Laplacian matrix L given in equation (3). In this paper, we present results for graphs with

$$z \in \{3, 4, 5, 10, 15, 20, 25, 30, 35, 40, 45, 50\}$$
$$n \in \{200, 300, 400, 500, 1000, 2000, 3000, 4000, 5000, 10\,000\}$$

where z and n have been chosen with an eye towards exploring their interdependence for large graphs. All averages are performed over a set containing N_G graph realizations, with $N_G = 5000$ for $n < 5000$ and $N_G = 1000$ graphs for $n \geqslant 5000$. The exact number of unique graphs, $\mathcal{N}_G$ with a given n and z grows quickly with n but is unknown in general. An asymptotic result for degrees satisfying $z \leqslant \sqrt{2\log n} - 1$ was proved by Bollobás in [34]. Explicit counts for small n and z can be found at the online encyclopedia of integer sequences [35], e.g. for $z = 3$ and $n = 16$, $\mathcal{N}_G = 4060$.

We begin our analysis by describing the eigenvalue distribution of L. For $n \gg 1$, the limiting form of the density of states $\rho(\varepsilon)$, the probability of an eigenvalue falling between ε and $\varepsilon + \mathrm{d}\varepsilon$, is given by the Kesten–McKay law [15, 16, 20]:

$$\rho(\varepsilon) = \frac{1}{n}\delta(\varepsilon) + \frac{z}{2\pi} \frac{\sqrt{4(z-1) - (\varepsilon - z)^2}}{z^2 - (\varepsilon - z)^2}; \quad |\varepsilon - z| \leqslant 2\sqrt{z-1}. \tag{5}$$

For finite values of n, Metz *et al* have recently computed the $1/n$ corrections to this expression, originating from the contributions of loops of all possible lengths.

For a graph with n vertices, the eigenvalues of the Laplacian matrix $\{\varepsilon_i\}$ are determined by exact diagonalization, and a comparison to equation (5) can be made by numerically constructing the histogram:

$$\langle \rho(\varepsilon) \rangle = \left\langle \frac{1}{n} \sum_{i=1}^{n} \delta(\varepsilon - \varepsilon_i) \right\rangle \tag{6}$$

where an average over N_G graph realizations is indicated by the angle brackets: $\langle \cdots \rangle \equiv (1/N_G) \sum_G (\cdots)$. The results for $n = 1000$, $z = 3, 4, 5, 10, 20, 50$ and $N_G = 5000$
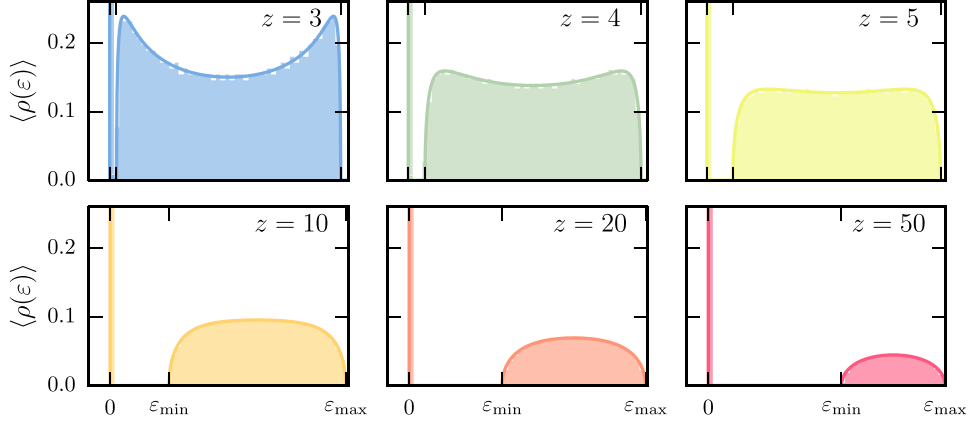
Figure 2. The probability of graph Laplacian eigenvalues for $n = 1000$ vertices with degrees $z = 3, 4, 5, 10, 20, 50$ computed by diagonalizing numerically constructed graphs (shaded region) compared with the large-n limit Kesten-McKay law defined in equation (5) (solid line). Eigenvalues in the continuum are bounded between $\varepsilon_{\min} = z - 2\sqrt{z-1}$ and $\varepsilon_{\max} = z + 2\sqrt{z-1}$, while the Perron–Frobenius mode with weight $1/n$ is shown as a spike at $\varepsilon = 0$.

are shown in figure 2. We observe only small graph-to-graph variations and find excellent agreement with the Kesten–McKay semi-circle law of equation (5) using 50 eigenvalue bins (solid line). For $n > 1000$ there is no visible discrepancy on this scale between the numerical results and the prediction for the large n limit. For finite sized random regular graphs, the spectrum of the Laplacian consists of a single eigenvalue at $\varepsilon = 0$ separated by a z-dependent gap [36] to a quasi-continuum of eigenvalues bounded between $\varepsilon_{\min} = z - 2\sqrt{z-1}$ and $\varepsilon_{\max} = z + 2\sqrt{z-1}$.

3. The inverse participation ratio

Less is understood about the set of eigenvectors $E = \{x \ : \ Lx = \varepsilon x\}$ [17, 27, 28] although for certain classes of regular graphs with $z \sim \mathrm{O}(n)$, they are believed (with high probability [18]) to be delocalized—meaning they have many non-zero components. The eigenvalue $\varepsilon = 0$ with weight $1/n$ in equation (5) and figure 3 corresponds to the special case of the Perron–Frobenius mode: $\wp \equiv (1/\sqrt{n}, \ldots, 1/\sqrt{n})$ and via orthogonality it follows that $x \cdot \wp = \sum_i x_i = 0$ for any eigenvector $x \neq \wp$. We wish to develop an understanding of the properties of the remaining eigenvectors $\mathcal{E} \equiv E \setminus \{\wp\}$, and in particular, determine how the non-zero elements of an arbitrary $x \in \mathcal{E}$ are distributed amongst its n coordinates.

To this end, we study the notion of *localization* of an eigenvector using the inverse participation ratio. Historically, the participation ratio p was introduced to aid in classifying the properties of atomic vibrations in disordered lattices [37]. It describes the fraction of the total number of sites which *participate* in a given normal mode vibration corresponding to the eigenvector $x = (x_1, \ldots, x_n) \in \mathbb{R}^n$ and takes the value

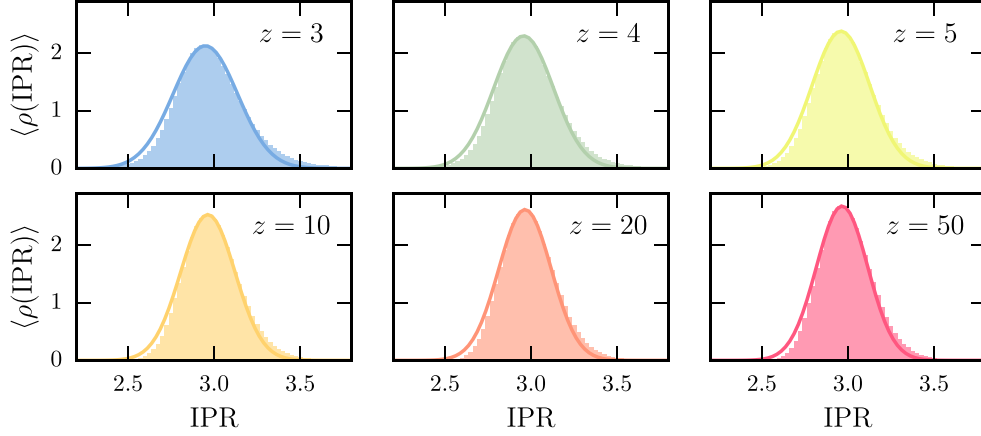$$p(x) = \frac{(\mu^1)^2}{\mu^0 \mu^2} \tag{7}$$

Figure 3. Histograms of IPR values for the Laplacian matrix on random regular graphs with $n = 1000$ vertices and degrees $z = 3, 4, 5, 10, 20, 50$. Solid lines represent fits to a Gaussian distribution.

where $\mu^r = \sum_{i=1}^{n} |x_i|^{2r}$ can be thought of as the rth moment of the kinetic energy of the mode. If a given normal mode only involves the motion of a single atom, it is characterized as *localized* and has $p = 1/n$. A vibrational mode consisting of all atoms participating equally is called *extended* and has $p = 1$. An equivalent measure was employed by Visscher [38] to study the degree of localization of electronic eigenstates in the Anderson model [2] with implications for the existence of a metal-insulator (delocalization-localization) transition in the presence of disorder.

When considering normalized eigenvectors $\boldsymbol{x} \cdot \boldsymbol{x} = ||\boldsymbol{x}|| = 1$, it is often more convenient to consider the associated inverse participation ratio (IPR):

$$\frac{1}{p(\boldsymbol{x})} \equiv \mathrm{IPR}(\boldsymbol{x}) = n \sum_{i=1}^{n} x_i^4. \tag{8}$$

For the Laplacian matrix in equation (3) with $\boldsymbol{x} \in E$ we have

$$1 \leqslant \mathrm{IPR}(\boldsymbol{x}) \leqslant \frac{n}{2} \tag{9}$$

with bounds corresponding to the extended Perron–Frobenius (lower bound) and localized (upper bound) modes, respectively. The finite size scaling of $\mathrm{IPR}(\boldsymbol{x})/n$ as $n \to \infty$ provides information on the existence of a mobility edge, which defines the portion of the spectrum with robust delocalized states. This scaling has been extensively studied for a large class of random matrices [39–42].

The inverse participation ratio thus provides a convenient single scalar value measuring the degree to which a particular eigenvector is localized ($p^{-1} \sim \mathrm{O}(n)$) or extended ($p^{-1} \sim \mathrm{O}(1)$). To obtain information on the reduced set of Laplacian eigenvectors $\mathcal{E}$ corresponding to non-zero eigenvalues, we construct a histogram of values in analogy with equation (6). The non-linear form of the IPR necessitates that the order of averaging is important, and we must compute

$$\rho(\mathrm{IPR}) = \frac{1}{n-1} \sum_{\boldsymbol{x} \in \mathcal{E}} \delta(\mathrm{IPR} - \mathrm{IPR}(\boldsymbol{x})) \tag{10}$$

for each graph realization separately before averaging over graphs. The resulting graph averaged distributions are shown in figure 3 for $n = 1000$, $z = 3, 4, 5, 10, 20, 50$ and $N_G = 5000$. The solid lines show the results of a fit to a Gaussian distribution for each n and z and there are clear deviations which skew to larger IPR values, most notably for small z. For fixed n, increasing z decreases the width of the distribution, and slightly improves the residual of the Gaussian fit, but quite strikingly, the mean stays at a value that is numerically very close to 3, with the result appearing to be exact as $n \to \infty$.

This empirical finding warrants an explanation, which we provide subsequently in section 4. In order to motivate our approach, we appeal to progress in understanding the statistics of eigenvectors in the more general setting of random matrix theory. Recently, Bourgade *et al* [32] and Backhausz and Szegedy [33] undertook a systematic study of eigenvector statistics of sparse random matrices. They recovered specific information about the eigenvectors of adjacency matrices of random regular graphs whose degree z is bounded by the number of vertices n. Mirroring the hypothesis in [32], let $\delta > 0$ be an arbitrarily small constant. For a random z-regular graph which satisfies $n^{\delta} \leqslant z \leqslant n^{2/3-\delta}$ their main result, theorem 1.1, implies that the entries of those eigenvectors of random regular graphs which are orthogonal to the Perron–Frobenius mode $\wp$ have asymptotically independent Gaussian distributed entries. Moreover, it is well-known that vectors whose entries are independently identically Gaussian distributed are uniformly distributed on the unit sphere. (See the textbook of Cramér [43, chapter 24] and the algorithmic implementation of this fact by Muller [44].) Together, these results suggest that the statistics of the inverse participation ratio can be directly investigated by computing moments of the IPR function using the uniform probability distribution on a subsphere which is orthogonal to $\wp$.

4. Analysis of the IPR on a hypersphere

In the previous section we numerically investigated the distribution of IPR values for all non Perron–Frobenius eigenvectors of each graph Laplacian across a large ensemble of graphs and empirically observed that for $n \gg 1$:

$$\left\langle \frac{1}{n-1} \sum_{x \in \mathcal{E}} \text{IPR}(x) \right\rangle \approx 3. \tag{11}$$

This result can be understood by exploiting the geometry of the set of eigenvectors $\mathcal{E} = E \smallsetminus \{\wp\}$ of each graph. Their terminal points lie on a hypersphere $S(\wp)$ which is orthogonal to the Perron–Frobenius mode $\wp$, and is a subsphere of the standard real unit sphere $S = \{u \in \mathbb{R}^n : ||u|| = 1\}$. In order to study the properties of the inverse participation ratio on a space containing $\mathcal{E}$, we observe that the function $\text{IPR}(x)$ is just a polynomial of n variables x_i composed from the sum of fourth order monomials $\text{IPR}(x) = n(x_1^4 + \cdots + x_n^4)$ which maps points $x \in S(\wp) \subset \mathbb{R}^n$ to $\mathbb{R}$. As described above, for random regular graphs with large n, the x_i can be taken to be independent and identically distributed according to the normal distribution [32, 33] and thus the vectors $x \in \mathcal{E}$ tend towards being uniformly distributed on $S(\wp)$. Thus in the limit of large n, the eigenvector and graph averages in equation (11) can be approximated by the continuous expectation value:

$$\mu_{\text{IPR}}^1 \equiv \langle \text{IPR} \rangle_{S(\wp)} = \int_{S(\wp)} \text{IPR}(x) P(x) \mathrm{d}\sigma(\wp) \tag{12}$$

where $d\sigma(\wp)$ is the measure and $P(\boldsymbol{x})$ the uniform distribution on $S(\wp)$:

$$P(\boldsymbol{x}) = \frac{1}{\int_{S(\wp)} d\sigma(\wp)} \ . \tag{13}$$

Similarly the second moment, μ_{IPR}^2, corresponding to the variance of the IPR distributions in figure 3 can be investigated by averaging the eighth order polynomial $[\text{IPR}(\boldsymbol{x})]^2$ on $S(\wp)$ and employing the usual identity

$$\mu_{\text{IPR}}^2 \equiv \left\langle (\text{IPR})^2 \right\rangle_{S(\wp)} - \left(\mu_{\text{IPR}}^1 \right)^2 \ . \tag{14}$$

Using equations (13) in (12) and (14) thus allows us to compute the continuous first and second moments of the inverse participation ratio via the integration of fourth and eighth order polynomials on $S(\wp)$. This can be accomplished using the short note of Folland [45] which provides a formula for integrating a polynomial over a sphere. Folland's formula is stated for a monomial $x^{\mathbf{a}} = x_1^{a_1} \cdots x_n^{a_n}$ and extends linearly to polynomials $\sum_{\mathbf{a}} c_{\mathbf{a}} \cdot x^{\mathbf{a}}$ with numerical coefficients $c_{\mathbf{a}}$. Furthermore, the integral of a monomial is dependent only on the Gamma function $\Gamma(b) = \int_0^\infty t^{b-1} e^{-t} \, dt$ where b is a complex number with positive real part. To proceed, write $d\sigma$ for the surface measure on the unit sphere $S \subset \mathbb{R}^n$. Folland's result is the following.

Theorem 1 ([45]). *Let* $x^{\mathbf{a}} = x_1^{a_1} \cdots x_n^{a_n}$ *be a monomial, so that* $a_j \geqslant 0$ *for all* $1 \leqslant j \leqslant n$. *Setting* $b_j = \frac{1}{2}(a_j + 1)$,

$$\int_S x^{\mathbf{a}} \, d\sigma = \begin{cases} 0 & \text{if some } a_j \text{ is odd,} \\[2mm] \frac{2\Gamma(b_1)\Gamma(b_2)\cdots\Gamma(b_n)}{\Gamma(b_1+b_2+\cdots+b_n)} & \text{if all } a_j \text{ are even.} \end{cases}$$

We wish to average the polynomial $\text{IPR}(\boldsymbol{x})$ over the subsphere $S(\wp) \subset S$ that is orthogonal to the Perron–Frobenius vector $\wp$. Thus, in order to use theorem 1 we must first rotate our subsphere $S(\wp)$ around a $(n-2)$-dimensional subspace to coincide with the subsphere $S(\boldsymbol{e}_n)$ as depicted for the case $n = 3$ in figure 4.

Note that although the target sphere $S(\boldsymbol{e}_n)$ is defined by coordinates in $\mathbb{R}^n$, the nth coordinate of each of its points equals zero. Hence, $S(\boldsymbol{e}_n)$ is realized as the unit sphere of $\mathbb{R}^{n-1}$ which is embedded in $\mathbb{R}^n$ according to the rule $(y_1, \ldots, y_{n-1}) \mapsto (y_1, \ldots, y_{n-1}, 0)$. Changing variables therefore allows the direct application of theorem 1 to the unit sphere in $\mathbb{R}^{n-1}$ to achieve our result. The remainder of this section is devoted to these analytic calculations.

4.1. The rotation matrix Q

The required change of variables is performed via a rotation matrix $Q \in \text{SO}(n)$ which has the property that for any $\boldsymbol{y} \in S(\boldsymbol{e}_n)$ there exists $\boldsymbol{x} \in S(\wp)$ such that

$$\boldsymbol{y} = Q\boldsymbol{x}. \tag{15}$$

We begin the construction of Q by using the Gram–Schmidt process to find two orthonormal vectors in the plane defined by $\boldsymbol{e}_n$ and $\wp$:

$$\boldsymbol{v}_1 = \wp = \frac{(1, \ldots, 1)}{\sqrt{n}} \tag{16}$$

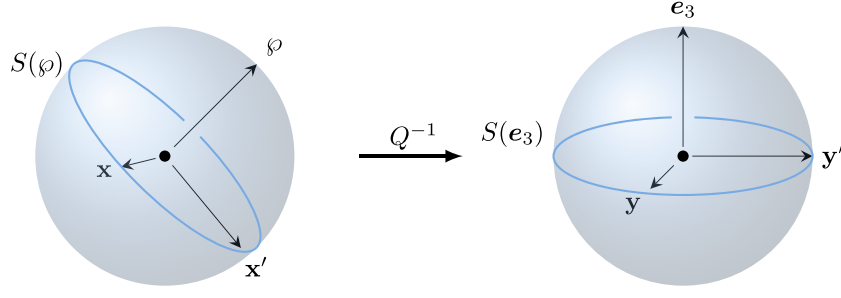**Figure 4.** The rotation procedure for $n = 3$ from an oriented to standard subsphere (circle) embedded in $\mathbb{R}^3$.

$$v_2 = \frac{e_n - (\wp \cdot e_n)\,e_n}{||e_n - (\wp \cdot e_n)\,e_n||} = -\frac{(1, \ldots, 1, 1 - n)}{\sqrt{n(n-1)}}. \tag{17}$$

To align $\wp$ with e_n, we need to perform a rotation by an angle θ defined by:

$$\cos \theta = \wp \cdot e_n = \frac{1}{\sqrt{n}} \tag{18}$$

around the plane formed by v_1 and v_2 and the identity space spanned by the $(n-2)$-dimensional complement of the orthonormal basis. Hence, we have

$$Q = \mathbb{1} + \sin \theta \, (v_2 \otimes v_1 - v_1 \otimes v_2) + (\cos \theta - 1)(v_1 \otimes v_1 + v_2 \otimes v_2) \tag{19}$$

where $\mathbb{1}$ is the $n \times n$ identity matrix and $\otimes$ represents the tensor product of vectors. Considering vector components: $v_{1i} = 1/\sqrt{n}$ and $v_{2i} = (n\delta_{ni} - 1)/\sqrt{n(n-1)}$ we express the rotation matrix in a form more useful for performing explicit calculations:

$$Q_{ij} = \delta_{ij} + \frac{1}{\sqrt{n}} \left[\frac{1 - \sqrt{n}}{n-1} (1 - \delta_{in} - \delta_{nj} + n\delta_{nj}\delta_{in}) + \delta_{in} - \delta_{nj} \right]. \tag{20}$$

Using equation (20) it is therefore straightforward to confirm that:

$$(i) \ \sum_{j=1}^{n} Q_{ij} = \sqrt{n}\delta_{in}, \ \text{and}$$

$$(ii) \ \forall \, x \in \mathbb{R}^n \text{ such that } ||x|| = 1 \text{ and } x \cdot \wp = 0, \ y_n = \sum_{j=1}^{n} Q_{nj}x_j = 0 \ .$$

4.2. Evaluation of the inverse participation ratio moments

Folland's straightforward application of theorem 1 shows that the $(n-2)$-dimensional measure of each of the spheres $S(e_n)$ and $S(\wp)$ is $2\pi^{(n-1)/2}/\Gamma(\frac{n-1}{2})$, whose reciprocal is $P(x)$, the probability of uniformly choosing a point from such a sphere. To proceed, write $d\sigma(e_n)$ for the $(n-2)$-dimensional surface measure of the sphere $S(e_n)$ and $d\sigma(\wp)$ for the $(n-2)$-dimensional surface measure of the sphere $S(\wp)$. Applying the multivariable change of basis formula for integrals to equation (12) therefore yields

$$\langle \mathrm{IPR} \rangle_{S(\wp)} = \int_{S(\wp)} \mathrm{IPR}(\boldsymbol{x}) \, \frac{\Gamma(\frac{n-1}{2})}{2\pi^{(n-1)/2}} \, \mathrm{d}\sigma(\wp)$$

$$= \frac{\Gamma(\frac{n-1}{2})}{2\pi^{(n-1)/2}} \int_{S(\boldsymbol{e}_n)} \mathrm{IPR}\left(Q^{-1}\boldsymbol{y}\right) \left| J\left(Q^{-1}\right) \right| \mathrm{d}\sigma(\boldsymbol{e}_n). \tag{21}$$

Note that Q is an orthonormal rotation matrix, so that the Jacobian $\left| J(Q^{-1}) \right| = 1$. As mentioned above, $y_n = 0$ since $\boldsymbol{y} \cdot \boldsymbol{e}_n = 0$, so that all our monomials have $(n-1)$ variables. Theorem 1 further guarantees that although the expansions of $\mathrm{IPR}(Q^{-1}\boldsymbol{y})$ and $[\mathrm{IPR}(Q^{-1}\boldsymbol{y})]^2$ have many monomial terms with odd exponents, our moment calculations give non-zero values for only those monomial terms having all their exponents even. Combining the structure of $Q^{-1} = Q^{\mathsf{T}}$, the multinomial theorem, the results of averaging relevant monomials $\langle y_k^{a_k} \cdots y_{k'}^{a_{k'}} \rangle_{S(\boldsymbol{e}_n)}$ over the sphere found in appendix A, and the expansions in appendix B we now give closed forms for the first and second moments of the inverse participation ratio over $S(\wp)$. Applying equation (21), the first moment is

$$\langle \mathrm{IPR} \rangle_{S(\wp)} = \frac{\Gamma(\frac{n-1}{2})}{2\pi^{(n-1)/2}} \int_{S(\boldsymbol{e}_n)} \mathrm{IPR}\left(Q^{-1}\boldsymbol{y}\right) \, \mathrm{d}\sigma(\boldsymbol{e}_n)$$

$$= n \sum_{i=1}^{n} \left(\sum_{k=1}^{n-1} \langle y_k^4 \rangle_{S(\boldsymbol{e}_n)} Q_{ki}^4 + 3 \sum_{k,\ell}^{n-1}{}' \langle y_k^2 y_\ell^2 \rangle_{S(\boldsymbol{e}_n)} Q_{ki}^2 Q_{\ell i}^2 \right)$$

$$= \frac{3n}{4} \frac{\Gamma(\frac{n-1}{2})}{\Gamma(\frac{n+3}{2})} \sum_{i=1}^{n} \left(\sum_{k=1}^{n-1} Q_{ki}^4 + \sum_{k,\ell}^{n-1}{}' Q_{ki}^2 Q_{\ell i}^2 \right) \tag{22}$$

where we have used the notation that a prime on a multiply indexed sum enforces the constraint that no equal indices are included, i.e.

$$\sum_{k,\ell}^{n-1}{}'(\cdots) \equiv \sum_{k \neq \ell}^{n-1}(\cdots) \equiv \sum_{k=1}^{n-1} \sum_{\ell=1}^{n-1}(\cdots) \left(1 - \delta_{k\ell}\right)$$

and the monomial averages over the subsphere $\langle y^4 \rangle_{S(\boldsymbol{e}_n)}$ and $\langle y^2 y^2 \rangle_{S(\boldsymbol{e}_n)}$ have been computed using theorem 1 with the individual results given in table A1. The double and triple summations over the components of the rotation matrix Q are evaluated in appendix B and substituting equations (B.3) and (B.4) into equation (22) yields:

$$\mu_{\mathrm{IPR}}^1 = \frac{3n}{(n+1)(n-1)} \left[n - \frac{29 + 30\sqrt{n} + 5n}{(1+\sqrt{n})^2} + \frac{24}{\sqrt{n}} - \frac{9}{n} \right.$$

$$\left. + \frac{(\sqrt{n}-1)(3\sqrt{n}+5)(n-2)}{n(\sqrt{n}+1)^2} \right]$$

$$= 3 - \frac{6}{n+1} \tag{23}$$

which has the observed limiting value of 3 for $n \gg 1$.

The calculation of the second central moment proceeds in a similar fashion by using equation (14) and applying the above general preliminaries to the square of the inverse participation ratio polynomial. We have

$$
\begin{aligned}
\left\langle \mathrm{IPR}^2 \right\rangle_{S(\wp)} &= \frac{\Gamma\left(\frac{n-1}{2}\right)}{2\pi^{(n-1)/2}} \int_{S(\boldsymbol{e}_n)} \left[\mathrm{IPR}\left(Q^{-1}\boldsymbol{y}\right) \right]^2 \, \mathrm{d}\sigma(\boldsymbol{e}_n) \\
&= n^2 \sum_{k=1}^{n-1} \left\langle y_k^8 \right\rangle_{S(\boldsymbol{e}_n)} \left[\sum_{i=1}^{n} Q_{ki}^8 + \sideset{}{'}\sum_{i,j}^{n} Q_{ki}^4 Q_{kj}^4 \right] \\
&\quad + n^2 \sideset{}{'}\sum_{k,\ell}^{n-1} \left\langle y_k^6 y_\ell^2 \right\rangle_{S(\boldsymbol{e}_n)} \left[28 \sum_{i=1}^{n} Q_{ki}^6 Q_{\ell i}^2 + \sideset{}{'}\sum_{i,j}^{n} \left(12 Q_{ki}^4 Q_{\ell j}^2 Q_{kj}^2 + 16 Q_{ki}^3 Q_{li} Q_{kj}^3 Q_{\ell j} \right) \right] \\
&\quad + n^2 \sideset{}{'}\sum_{k,\ell}^{n-1} \left\langle y_k^4 y_\ell^4 \right\rangle_{S(\boldsymbol{e}_n)} \left[35 \sum_{i=1}^{n} Q_{ki}^4 Q_{\ell i}^4 + \sideset{}{'}\sum_{i,j}^{n} \left(Q_{ki}^4 Q_{\ell j}^4 + 18 Q_{ki}^2 Q_{\ell i}^2 Q_{kj}^2 Q_{\ell j}^2 \right. \right. \\
&\quad \left. \left. + 16 Q_{ki}^3 Q_{\ell i} Q_{kj} Q_{\ell j}^3 \right) \right] \\
&\quad + n^2 \sideset{}{'}\sum_{k,\ell,m}^{n-1} \left\langle y_k^4 y_\ell^2 y_m^2 \right\rangle_{S(\boldsymbol{e}_n)} \left[210 \sum_{i=1}^{n} Q_{ki}^3 Q_{\ell i}^3 Q_{mi}^3 + \sideset{}{'}\sum_{i,j}^{n} \left(6 Q_{ki}^4 Q_{\ell j}^2 Q_{mj}^2 \right. \right. \\
&\quad \left. \left. + 72 Q_{ki}^2 Q_{\ell i} Q_{mi} Q_{kj}^2 Q_{\ell j} Q_{mj} + 96 Q_{ki}^3 Q_{\ell i} Q_{kj} Q_{\ell j} Q_{mj}^2 \right) \right] \\
&\quad + n^2 \sideset{}{'}\sum_{k,\ell,m,p}^{n-1} \left\langle y_k^2 y_\ell^2 y_m^2 y_p^2 \right\rangle_{S(\boldsymbol{e}_n)} \left[105 \sum_{i=1}^{n} Q_{ki}^2 Q_{\ell i}^2 Q_{mi}^2 Q_{pi}^2 + \sideset{}{'}\sum_{i,j}^{n} \left(9 Q_{ki}^2 Q_{\ell i}^2 Q_{mj}^2 Q_{pj}^2 \right. \right. \\
&\quad \left. \left. + 72 Q_{ki}^2 Q_{\ell i} Q_{mi} Q_{pj}^2 Q_{\ell j} Q_{mj} + 24 Q_{ki} Q_{\ell i} Q_{mi} Q_{pi} Q_{kj} Q_{\ell j} Q_{mj} Q_{pj} \right) \right]
\end{aligned}
\tag{24}
$$

and combining the results of table A2 and appendix B we find

$$
\left\langle \mathrm{IPR}^2 \right\rangle_{S(\wp)} = 9 + \frac{48}{n+1} - \frac{270}{n+3} + \frac{210}{n+5}.
\tag{25}
$$

Subtracting the square of the first moment, we arrive at the final expression for the second moment of the inverse participation ratio on $S(\wp)$

$$
\mu_{\mathrm{IPR}}^2 = \frac{24n(n-2)(n-3)}{(n+5)(n+3)(n+1)^2}
\tag{26}
$$

which indeed tends to zero as $n \to \infty$.

5. Comparison with exact diagonalization results

Having uncovered the origin of the universal number 3 as $\lim_{n\to\infty} \mu_{\mathrm{IPR}}^1$ for the mean of the continuous IPR, we now undertake a systematic comparison of exact diagonalization results for the inverse participation ratio of the Laplacian on finite sized random regular graphs and the predictions on subspheres embedded in $\mathbb{R}^n$ as a function of z and n.
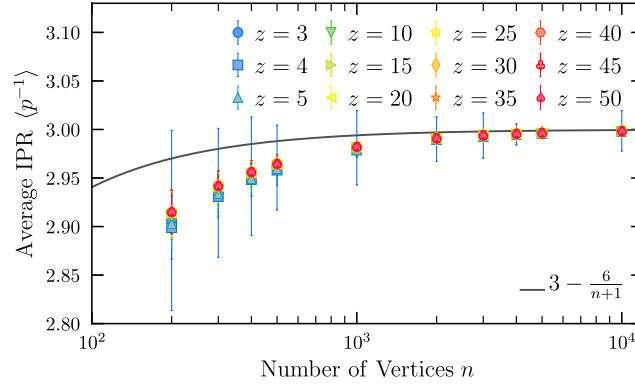
Figure 5. Graph and mode averaged inverse participation ratio versus the number of vertices n for different graph degrees z (symbols). The solid line shows the finite size prediction for μ_{IPR}^1 obtained by averaging over a sphere.

5.1. 1st IPR moment

The finite size scaling behavior of the first moment of the IPR can be quantified by explicitly computing the average of the IPR over all non-Perron–Frobenius eigenvectors $\boldsymbol{x} \in \mathcal{E}$, and then further averaging this quantity over graph realizations. In particular, we define the mode-averaged IPR (first IPR moment) for a given graph to be

$$p^{-1} = \frac{1}{n-1} \sum_{\boldsymbol{x} \in \mathcal{E}} \text{IPR}(\boldsymbol{x}), \tag{27}$$

while $\langle p^{-1} \rangle$ includes an additional average over the graph ensemble. Figure 5 depicts the n dependence of this quantity for all graph degrees considered, where we have averaged over $N_G = 5000$ random regular graphs for $n < 5000$ and $N_G = 1000$ graphs for $n \geqslant 5000$.

The solid line describes the function $\mu_{IPR}^1 = 3 - 6/(n+1)$ derived in equation (23) by averaging the IPR polynomial over the subsphere $S(\wp)$. There is good agreement for $n > 1000$, seemingly independent of graph degree. The error bars are obtained by computing the standard deviation of p^{-1} over all graphs in the generated set, with the largest uncertainties occurring for $z = 3$. We postpone a discussion of the size and z-dependence of graph-to-graph fluctuations until the end of this section.

We may investigate deviations between $\langle p^{-1} \rangle$ and μ_{IPR}^1 by defining a normalized residual

$$\Delta_1(z,n) = 1 - \frac{\langle p^{-1} \rangle}{\mu_{IPR}^1} \tag{28}$$

which is plotted in figure 6 (left) as a function of n for different values of z. The residual decays with increasing z and n with the correction being fit by an empirically determined function of the form $c_0(z) + c_1(z)/n$ (dashed line) where the extracted coefficients are shown in the right panel of figure 6. The exact diagonalization data is consistent with the absence of any $O(1)$ correction to equation (23) for large z within errorbars, i.e. $c_0(z \to \infty) \to 0$. The coefficient $c_1(z)$ appears to decay only weakly with increasing z and a z-dependent $1/n$ correction cannot be ruled out at the level of our statistical uncertainty for $n \leqslant 1000$. For $n \geqslant 1000$ the residual can also be described by a function of the form $c_{3/2}(z)/n^{3/2}$ as shown by the solid line in figure 6 (left) supporting the leading finite n behavior of μ_{IPR}^1.
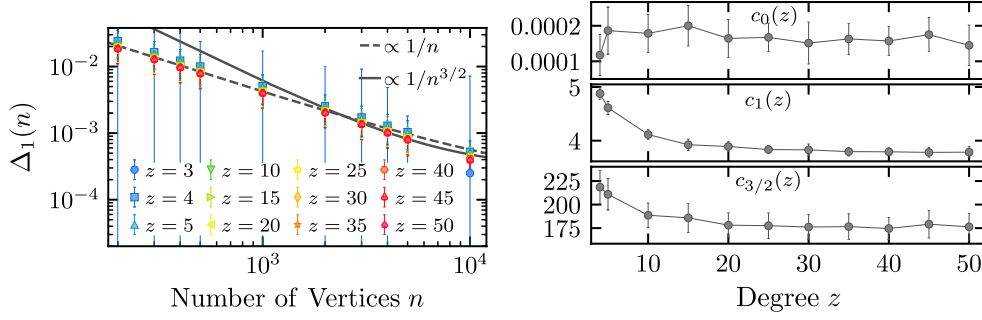
Figure 6. Left: Normalized deviation of the graph and mode averaged inverse participation ratio for the Laplacian on random regular graphs from the sphere averaged value of μ_{IPR}^1, given in equation (28) in the text. Two fits to the residual data corresponding to $c_0 + c_1/n$ (dashed) and $c_{3/2}/n^{3/2}$ (solid) are shown with the latter only using data with $n > 1000$. Right: z-dependent fitting parameters are consistent with vanishing $O(1)$ corrections to to μ_{IPR}^1.

5.2. 2nd IPR moment

Next, we consider the prediction of equation (26) by studying the second moment of the distribution of IPR values on finite sized random regular graphs: $\left\langle (p^{-1})^2 \right\rangle - \left\langle p^{-1} \right\rangle^2$ averaged over $N_G = 5000$ unique graphs for $n < 5000$ and $N_G = 1000$ for $n \geqslant 5000$. The results are shown in figure 7, where now deviations from the sphere-averaged value μ_{IPR}^2 (included as a solid line) are observed for all values of n and z considered.

The degree dependence is the most obvious: the exact diagonalization results are systematically larger than μ_{IPR}^2 for small z, with the discrepancy decreasing as z increases. We have not included data for $z = 3$ in figure 7 as these points lie mostly off the scale and the peculiarities of this degree will be carefully investigated in the following subsection. Additionally, due to the logarithmic scale, we have only plotted errorbars showing the additive uncertainty across graphs. For $z > 4$, the standard deviation is on the order of the symbol sizes.

We again define a normalized residual for the second moment:

$$\Delta_2(z, n) = 1 - \frac{\left\langle (p^{-1})^2 \right\rangle - \left\langle p^{-1} \right\rangle^2}{\mu_{\mathrm{IPR}}^2} \tag{29}$$

and the absolute value $|\Delta_2(z, n)|$ is plotted in figure 8.

Here, the dominant deviations from the first sphere averaged value μ_{IPR}^1 are degree dependent, and they can be described by a function of the form $c_2^0 + c_2^1/z + c_2^2/z^2$. The values of the fitting constants c_2^k depend on n, with the solid line in the left panel representing their average values for $n > 1000$. Different fitting functions were investigated, including those with non-integer negative powers of z, but the resulting second order polynomial in $1/z$ provided the optimal value of the least square fitting χ^2 value. The right panel of figure 8 shows the n dependence of Δ_2 and it appears that it remains non-zero even as $n \to \infty$. This is consistent with the fitting parameter c_0^2 which is finite within errorbars for all values of z considered.

5.3. Effects of localized eigenvectors

We now address the issue of the large graph-to-graph variance observed around the first and second moments of the IPR distribution for small z. This data is displayed in figure 9 where
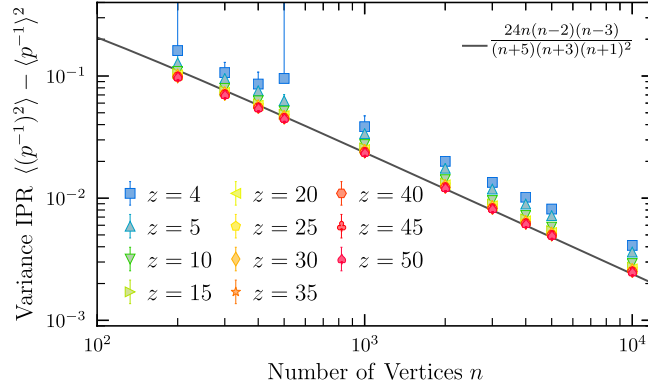
Figure 7. The graph averaged second moment of the mode averaged inverse participation ratio distribution for random regular graphs of varying degree versus the number of vertices. The solid line shows the sphere averaged value, μ_{IPR}^2.
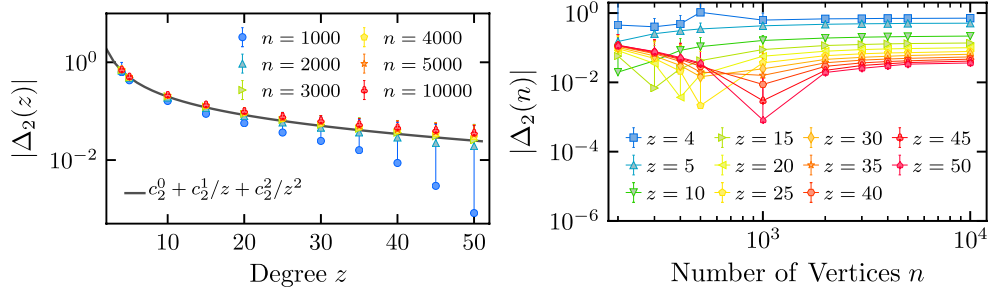

Figure 8. The normalized positive residual between the second moment of the inverse participation ratio distribution for large random regular graphs and the value obtained by averaging over a sphere. The left panel shows that the z dependence of the correction can be fit via a second order polynomial in $1/z$ with an offset that persists in the $n \to \infty$ limit (right panel).

the graph averaged first and second moments of the IPR distribution are shown as a function of n for $z = 3$. The displayed errorbars correspond to one standard deviation and we observe that the effects are most pronounced for the variance of the IPR. Data points consistently fall above the sphere averaged value of μ_{IPR}^2, and the mean value between graphs can vary by as much as 1000%. However, for both the first and second moments, the data is consistent with values of μ_{IPR}^1 and μ_{IPR}^2 computed using integration. The existence of a single outlying data point corresponding to $n = 5000$ that is much closer to μ_{IPR}^2 in the right panel of figure 9 is suggestive that the sample set of unique random regular graphs may not be large enough to capture the variation in the eigenvector components amongst graphs as measured by the inverse participation ratio.

To better understand the prevalence of this effect for graphs of small degree, we have exactly diagonalized the Laplacian for every one of the $\mathcal{N}_G = 4060$ unique random regular graphs with $n = 16$ and $z = 3$ [46]. Analyzing the eigenvectors and computing the inverse participation ratio, we find:

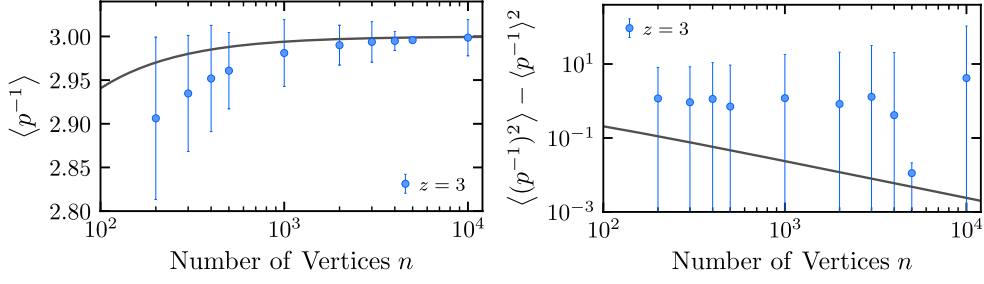$$\langle p^{-1} \rangle = 2.4 \pm 0.4 \tag{30}$$

Figure 9. The first (left) and second (right) moments of the inverse participation ratio distribution versus the number of vertices computed via exact diagonalization of 5000 random regular graphs with degree $z = 3$. The errorbars correspond to one standard deviation, and they are significantly larger than those observed for $z > 3$. Solid gray lines are the predicted sphere averaged values of μ_{IPR}^1 and μ_{IPR}^2 defined in equations (23) and (26) respectively.

$$\left\langle (p^{-1})^2 \right\rangle - \left\langle p^{-1} \right\rangle^2 = 0.95 \pm 1.2. \tag{31}$$

The origin of these sizeable graph-to-graph variations is uncovered in the left panel of figure 10, which shows a histogram of all IPR values (excluding the Perron–Frobenius mode) for the complete graph set plotted against their corresponding eigenvalue. The frequency of IPR values is shown on a logarithmic color scale from light to dark, and we observe two spikes near $\varepsilon = z$ and $\varepsilon = z + 1$ with the inverse participation ratio ranging up to its maximal value of $n/2 = 8$. In the right panel of figure 10 we show the maximum value of the IPR across all $n = 16$ modes and find at least one value of 8 for nearly 15% of graphs in the set.

These graph realizations contain special eigenvectors $\{v\} \subset \mathcal{E}$ of the Laplacian, with $\text{IPR}(v) = n/2$. More generally, a vector with exactly k equal non-zero sites is of the form

$$v_i = \frac{(-1)^{q_i}}{\sqrt{k}} \delta_{i,i(k)} \tag{32}$$

where $i(k) \in \{i_1, i_2, \cdots, i_{k-1}, i_k\}$ and $q_i \in \{0, 1\}$ such that $\sum_{i(k)} (-1)^{q_i} = 0$. Clearly this is only possible for $k = 2m$ where $m \in \{1, \cdots, \lfloor n/2 \rfloor\}$, with the total number of such vectors given by the multinomial coefficient

$$\binom{n}{m,\ m,\ n - 2m} = \frac{n!}{m!\ m!\ (n - 2m)!}.$$

For vectors of this form, the inverse participation ratio is given by

$$\text{IPR}(v) = n \sum_{i=1}^{n} |v_i|^4 = \frac{n}{k^2} k = \frac{n}{k} \tag{33}$$

which is exactly what we observe for $k = 2$. This maximal value for the IPR occurs for the most localized mode that is still compatible with orthonormality to the Perron–Frobenius eigenvector and consists of exactly two non-zero values with opposite sign. We have confirmed that such eigenvectors indeed appear in our large-n graph ensembles for $z = 3$. Such vectors have a maximal nodal domain count of unity [28] and we observe that almost all eigenvectors with $\text{IPR}(v) = n/2$ have non-zero components of opposite sign situated in vector components with consecutive indices.
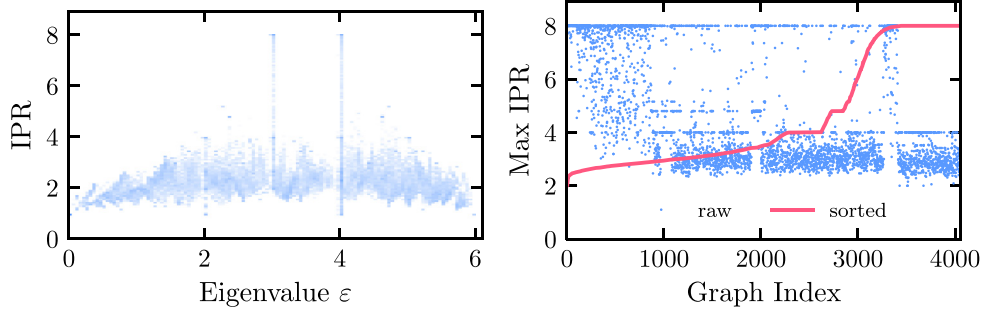
Figure 10. A histogram with shading on a logarithmic scale of the inverse participation ratio versus eigenvalue for all 4060 random regular graphs with $n = 16$ and $z = 3$ (left). The right panel shows the maximum value of the inverse participation ratio across all modes for a given graph plotted as a function of a fictitious graph index. By relabeling the graph index we also include the maximum value sorted by size.

The large graph-to-graph variations displayed in figure 9 can thus be traced back to these localized eigenvectors in combination with the prefactor of n in the definition of the IPR given in equation (8). By averaging over the sphere, we found in equation (23) that $\mu^1_{\mathrm{IPR}} \sim 3$ for $n \gg 1$. However as just demonstrated, localized eigenvectors can contribute IPR values of $O(n)$ to the first moment. This implies that the variance around the mean could contain dominant terms scaling like n^2 which will always have an effect when averaging over a finite number of large graphs.

6. Discussion

In this paper we have investigated the first and second moments of the distribution of the inverse participation ratio for all eigenvectors of the discrete Laplacian on finite size random regular graphs. By exactly diagonalizing large ensembles of graphs of up to $n = 10\,000$ vertices we find that the first moment of the inverse participation ratio approaches a constant of order unity $\lim_{n \to \infty} \langle p^{-1} \rangle = 3$ for all values of z. This result can be understood in terms of an analytically determined value for the average inverse participation ratio $\mu^1_{\mathrm{IPR}} = 3 - 6/(n + 1)$ obtained by averaging a fourth order polynomial corresponding to the IPR over the sphere $S(\wp)$ with uniform probability measure. We take this agreement as additional evidence that that the *average* eigenvector of the Laplacian on random regular graphs is delocalized, with its components tending towards being independent and identically distributed Gaussian random variables. For smaller values of n that do not necessarily satisfy the constraint $n^\delta \leqslant z \leqslant n^{2/3-\delta}$ for $\delta > 0$ [32], we observe deviations from μ^1_{IPR} at $O(1/n)$ that could be potentially useful when quantifying the distance from uniformity for a given set of random regular graph eigenvectors. The methodology used here to average the IPR polynomial over the hypersphere with constant probability could be employed to study other observables of physical interest on random graphs when n is large.

For the variance of the inverse participation ratio computed over all modes, we have again compared our exact random regular graph eigenvectors with an analytical result from continuous averaging over $S(\wp)$ with uniform measure where we find $\mu^2_{\mathrm{IPR}} = 24n(n - 2)(n - 3)/[(n + 5)(n + 3)(n + 1)^2]$. Here we observe weaker agreement that now strongly depends on the graph degree. This discrepancy appears to persist even in the limits $z, n \to \infty$. When computing the standard deviation of the IPR over an ensemble of up

to 5000 random regular graphs, we find that for small values of the graph degree z, large fluctuations between graph eigenvectors can cause variations in the first and second moments as large as 1000%. By analyzing the complete set of graphs for $z = 3$ and $n = 16$ we have shown that such deviations may arise from graphs where the Laplacian has localized eigenvectors consisting of only a few non-zero elements and thus IPR values of $n/2$. Although we have no proof that these vectors appear as eigenvectors of the Laplacian for finite size random regular graphs in general, we have demonstrated that there are factorially many such eigenvectors that are orthonormal to the Perron–Frobenius mode.

In general, the large but finite ensemble size of random regular graphs we analyze is much smaller than the total number of random regular graphs, which is known [34] to asymptotically grow exponentially with n. Hence, the fact that the standard deviation in the mean and variance of the inverse participation ratio for large n and z appear to be small is likely due to our samples of random regular graphs not being fully representative of the eigenvector variation which exists.

As z and n increase, extremely large ensembles of graphs need to be studied in order to to balance the dominant effects of localized modes, especially for non-linear observables. Thus, any observed deviation of the 2nd moment of the IPR from its uniform value for a given set of finite size graphs could be employed as a proxy for the representative suitability of the sampled set when n is large. This may may have practical implications for studying physical models with observables computed on regular graphs.

It would be interesting to explore this issue further, although considerable computational resources would have to be employed to diagonalize large numbers of graph Laplacians for $n \gg 1$. Determining the combinatorial, physical, and theoretical significance of these localized eigenvectors is thus left as a topic of future work.

Acknowledgments

Appendix A. Averages of monomials on the sphere

This appendix contains results of averaging monomials over the uniform distribution on $S(\boldsymbol{e}_n)$ necessary for the integral calculations of section 4. Note that in our case, the polynomial $\mathrm{IPR}(Q^{-1}\boldsymbol{y})$ consists of monomials in the variables $y_1, \ldots, y_{n-1}$ since $y_n = 0$. Theorem 1 guarantees that the integral of a monomial is non-zero precisely when its variables have even exponents, and as such, we give values in only this case.

When performing the first moment calculations we apply theorem 1 to two distinct monomial types. The monomial y_i^4 has $a_i = 4$ for a fixed i and $a_j = 0$ for all $j \neq i$, while the monomial $y_i^2 y_j^2$ has $a_i = a_j = 2$ and $a_k = 0$ for $k \neq i, j$. In the first case, we therefore have $b_i = 5/2$

Table A1. The average values of the degree four monomials with even exponents in $y_1, \ldots, y_{n-1}$ taken over the domain $S(e_n)$ with uniform probability.

Average:	$\langle y_k^4 \rangle_{S(e_n)}$	$\langle y_k^2 y_\ell^2 \rangle_{S(e_n)}$
Value:	$\frac{3}{4} \frac{\Gamma(\frac{n-1}{2})}{\Gamma(\frac{n+3}{2})}$	$\frac{1}{4} \frac{\Gamma(\frac{n-1}{2})}{\Gamma(\frac{n+3}{2})}$

Table A2. The average values of the degree eight monomials with even exponents in $y_1, \ldots, y_{n-1}$ taken over the domain $S(e_n)$ with uniform probability.

Average:	$\langle y_k^8 \rangle_{S(e_n)}$	$\langle y_k^6 y_\ell^2 \rangle_{S(e_n)}$	$\langle y_k^4 y_\ell^4 \rangle_{S(e_n)}$	$\langle y_k^4 y_\ell^2 y_m^2 \rangle_{S(e_n)}$	$\langle y_k^2 y_\ell^2 y_m^2 y_p^2 \rangle_{S(e_n)}$
Value:	$\frac{105}{16} \frac{\Gamma(\frac{n-1}{2})}{\Gamma(\frac{n+7}{2})}$	$\frac{15}{16} \frac{\Gamma(\frac{n-1}{2})}{\Gamma(\frac{n+7}{2})}$	$\frac{9}{16} \frac{\Gamma(\frac{n-1}{2})}{\Gamma(\frac{n+7}{2})}$	$\frac{3}{16} \frac{\Gamma(\frac{n-1}{2})}{\Gamma(\frac{n+7}{2})}$	$\frac{1}{16} \frac{\Gamma(\frac{n-1}{2})}{\Gamma(\frac{n+7}{2})}$

for a single i and $b_j = 1/2$ for $j \neq i$. In the second case, $b_i = b_j = 3/2$ and $b_k = 1/2$ for $k \neq i, j$. For y_k^4 we average over $S(e_n)$ and find:

$$
\begin{aligned}
\langle y_k^4 \rangle_{S(e_n)} &= \int_{S(e_n)} y_k^4 \, P(y) \, d\sigma(e_n) \\
&= \frac{\Gamma(\frac{n-1}{2})}{2\pi^{(n-1)/2}} \frac{2\Gamma(\frac{5}{2}) \left[\Gamma(\frac{1}{2}) \right]^{n-2}}{\Gamma(\frac{n+3}{2})} \\
&= \frac{3}{4} \frac{\Gamma(\frac{n-1}{2})}{\Gamma(\frac{n+3}{2})}.
\end{aligned}
\tag{A.1}
$$

This result along with the similarly computed $\langle y^2 y^2 \rangle$ term are gathered in table A1.

A similar analysis of the five monomial types appearing in the second moment's polynomial $[\text{IPR}(Q^{-1}y)]^2$ yields non-zero averages for those monomials of total degree eight which we list in table A2.

We now discuss each of the denominators appearing in these monomial integral calculations, and do so taking the value $\Gamma(\frac{n-1}{2})$ into account. This quantity is the numerator of the probability $P(x)$ of choosing points uniformly from the sphere and is a prefactor of each moment calculation. A closed form for the first and second IPR moments therefore depends on our ability to simplify several n-dependent ratios.

For the first moment, the total degree of the monomials is four, giving the denominator of theorem 1 a value of $\Gamma(\frac{n+3}{2})$. Hence, we seek a closed form for $\Gamma(\frac{n-1}{2})/\Gamma(\frac{n+3}{2})$. For a positive integer k, the Gamma function takes the values $\Gamma(k) = (k-1)!$ and $\Gamma(k + \frac{1}{2}) = (k - \frac{1}{2}) \cdots (\frac{1}{2})\sqrt{\pi}$ so that we have the following derivations:

If $n - 1 = 2k$ is even, then

$$
\frac{\Gamma(\frac{n-1}{2})}{\Gamma(\frac{n+3}{2})} = \frac{(k-1)!}{(k+1)!} = \frac{1}{(\frac{n+1}{2})(\frac{n-1}{2})} = \frac{4}{(n+1)(n-1)}.
\tag{A.2}
$$

On the other hand, if $n - 1$ is odd, then $n - 1 = 2k + 1$ for some k and

$$
\frac{\Gamma(\frac{n-1}{2})}{\Gamma(\frac{n+3}{2})} = \frac{(k - \frac{1}{2}) \cdots (\frac{1}{2})\sqrt{\pi}}{(k + \frac{3}{2})(k + \frac{1}{2}) \cdots (\frac{1}{2})\sqrt{\pi}} = \frac{4}{(2k+3)(2k+1)} = \frac{4}{(n+1)(n-1)}.
\tag{A.3}
$$

The second moment calculation contains only monomials of total degree eight, so that the denominator of theorem 1 is $\Gamma(\frac{n+7}{2})$. In a fashion similar to the derivation above, we give an alternate form for the fraction $\Gamma(\frac{n-1}{2})/\Gamma(\frac{n+7}{2})$.

When $n - 1 = 2k$ is even, we have

$$\frac{\Gamma(\frac{n-1}{2})}{\Gamma(\frac{n+7}{2})} = \frac{(k-1)!}{(k+3)!} = \frac{1}{(k+3)(k+2)(k+1)(k)} = \frac{16}{(n+5)(n+3)(n+1)(n-1)}. \tag{A.4}$$

On the other hand, for odd $n - 1 = 2k + 1$,

$$\frac{\Gamma(\frac{n-1}{2})}{\Gamma(\frac{n+7}{2})} = \frac{\left(k-\frac{1}{2}\right)\left(k-\frac{3}{2}\right)\cdots\left(\frac{1}{2}\right)\sqrt{\pi}}{\left(k+\frac{7}{2}\right)\left(k+\frac{5}{2}\right)\left(k+\frac{3}{2}\right)\cdots\left(\frac{1}{2}\right)\sqrt{\pi}} = \frac{16}{(n+5)(n+3)(n+1)(n-1)}. \tag{A.5}$$

Appendix B. Evaluation of *Q* summations

In this appendix we provide details on the evaluation of the summations over the components of the rotation matrix Q given in equation (20) that appear in the expressions for the first (equation (22)) and second (equation (24)) moments of the of the inverse participation ratio. These evaluations are performed by first noting that all such powers of Q only appear with the first index smaller than n and in this restricted case we can write:

$$(Q_{ij})^s = \frac{1}{(n+\sqrt{n})^s}\left[(-1)^s + \alpha_s(n)\delta_{nj} + \beta_s(n)\delta_{ij}\right] \tag{B.1}$$

where $\alpha_s(n)$ and $\beta_s(n)$ are power dependent functions of n that are listed in table B1 and we have used the fact that $\delta_{ij}^s = \delta_{ij}$ and $\delta_{ij}^s\delta_{n,j}^{s'} = 0 \;\forall s, s' \geqslant 1$ since $i < n$.

B.1. 1st IPR moment

We begin by using equation (B.1) to perform the double and triple summations appearing in the expression for the first moment of the inverse participation ratio in equation (22).

$$\sum_{i=1}^{n}\sum_{k=1}^{n-1} Q_{ki}^4 = \frac{1}{(n+\sqrt{n})^4}\sum_{i=1}^{n}\sum_{k=1}^{n-1}\left[1 + \alpha_4(n)\delta_{ni} + \beta_4(n)\delta_{ki}\right]$$

$$= \frac{1}{(n+\sqrt{n})^4}\left[n(n-1) + \alpha_4(n)(n-1) + \beta_4(n)(n-1)\right] \tag{B.2}$$

$$= \frac{n-1}{(n+\sqrt{n})^4}\left[n + \alpha_4(n) + \beta_4(n)\right]$$

and using the values of $\alpha_4(n)$ and $\beta_4(n)$ in table B1 we find

$$\sum_{i=1}^{n}\sum_{k=1}^{n-1} Q_{ki}^4 = n - \frac{29 + 30\sqrt{n} + 5n}{(1+\sqrt{n})^2} + \frac{24}{\sqrt{n}} - \frac{9}{n}. \tag{B.3}$$

Now, dropping the explicit n dependence of the α_s and β_s functions for simplicity, the triple summation may be performed in a similar manner:

Table B1. Expressions for $\alpha_s(n)$ and $\beta_s(n)$ appearing as coefficients of Kronecker δ-functions when evaluating powers of the components of the rotation matrix $(Q_{ij})^s$ where $i < n$ in equation (B.1).

s	$\alpha_s(n)$	$\beta_s(n)$
1	$-\sqrt{n}$	$n + \sqrt{n}$
2	$n + 2\sqrt{n}$	$(n-1)(n+2\sqrt{n})$
3	$-\sqrt{n}\,(3 + 3\sqrt{n} + n)$	$(n+\sqrt{n})(3 - 3\sqrt{n} - 2n + 2n^{3/2} + n^2)$
4	$(n + 2\sqrt{n})(2 + 2\sqrt{n} + n)$	$(n-1)(n+2\sqrt{n})$ $\times (n^2 + 2n^{3/2} - n - 2\sqrt{n} + 2)$
6	$(n + 2\sqrt{n})(1 + \sqrt{n} + n)$ $\times (3 + 3\sqrt{n} + n)$	$(n + 2\sqrt{n})(n-1)(1 - \sqrt{n} + 2n^{3/2} + n^2)$ $\times (3 - 3\sqrt{n} - 2n + 2n^{3/2} + n^2)$
8	$(n + 2\sqrt{n})(2 + 2\sqrt{n} + n)$ $\times (2 + 4\sqrt{n} + 6n + 4n^{3/2} + n^2)$	$(n + 2\sqrt{n})(n-1)$ $\times (2 - 2\sqrt{n} - n + 2n^{3/2} + n^2)$ $\times (2 - 4\sqrt{n} + 2n + 8n^{3/2} - 5n^2$ $- 8n^{5/2} + 2n^3 + 4n^{7/2} + n^4)$

$$
\begin{aligned}
\sum_{i=1}^{n} \sideset{}{'}\sum_{k,\ell}^{n-1} Q_{ki}^2 Q_{\ell i}^2 &= \frac{1}{(n+\sqrt{n})^4} \sum_{i=1}^{n} \sum_{k\neq\ell}^{n-1} \left(1 + \alpha_2 \delta_{ni} + \beta_2 \delta_{ki}\right)\left(1 + \alpha_2 \delta_{ni} + \beta_2 \delta_{\ell i}\right) \\
&= \frac{1}{(n+\sqrt{n})^4} \sum_{k\neq\ell}^{n-1} \left[(1+\alpha_2)^2 + \sum_{i=1}^{n-1}(1+\beta_2\delta_{ki})(1+\beta_2\delta_{\ell i})\right] \\
&= \frac{1}{(n+\sqrt{n})^4} \sum_{k\neq\ell}^{n-1} \left[(1+\alpha_2)^2 + n - 1 + 2\beta_2\right] \\
&= \frac{(n-1)(n-2)}{(n+\sqrt{n})^4} \left[(1+\alpha_2)^2 + n - 1 + 2\beta_2\right] \\
&= \frac{(\sqrt{n}-1)(3\sqrt{n}+5)(n-2)}{n(\sqrt{n}+1)^2},
\end{aligned}
\tag{B.4}
$$

where we have used $\alpha_2(n)$ and $\beta_2(n)$ from table B1.

B.2. 2nd IPR moment

There are seventeen individual summations appearing in the expression for the average of the square of the inverse participation ratio over the sphere given in equation (24) and we will include the details of only a representative sample here. All can be performed using similar techniques employing equation (B.1) and table B1 and we begin with the sum over the components of Q^8 which can be evaluated in exact analogy with equation (B.2):

$$
\begin{aligned}
\sum_{k=1}^{n-1} \sum_{i=1}^{n} Q_{ki}^8 &= \frac{1}{(n+\sqrt{n})^8} \sum_{k=1}^{n-1} \sum_{i=1}^{n} \left[1 + \alpha_8 \delta_{ni} + \beta_8 \delta_{ki}\right] \\
&= \frac{\sqrt{n}-1}{(1+\sqrt{n})^6 n^3} \Big(49 + 7\sqrt{n} - 7n + 119n^{3/2} + 21n^2 - 133n^{5/2} + 9n^3 \\
&\qquad + 111n^{7/2} + n^4 - 57n^{9/2} - 13n^5 + 13n^{11/2} + 7n^6 + n^{13/2}\Big).
\end{aligned}
$$

The next novel term includes Q^6 which appears as the third summation and is evaluated in a similar method as in equation (B.4) albeit with the modification that it involves the product of two different powers of Q:

$$\sum_{k,\ell}' \sum_{i=1}^{n} Q_{ki}^6 Q_{\ell i}^2 = \frac{1}{(n+\sqrt{n})^8} \sum_{k\neq\ell}^{n-1} \sum_{i=1}^{n} (1 + \alpha_6\delta_{ni} + \beta_6\delta_{ki})(1 + \alpha_2\delta_{ni} + \beta_2\delta_{\ell i})$$

$$= \frac{1}{(n+\sqrt{n})^8} \sum_{k\neq\ell}^{n-1} \left[(1+\alpha_6)(1+\alpha_2) + \sum_{i=1}^{n-1}(1+\beta_6\delta_{ki})(1+\beta_2\delta_{\ell i}) \right]$$

$$= \frac{(n-1)(n-2)}{(n+\sqrt{n})^8} \left[(1+\alpha_6)(1+\alpha_2) + n - 1 + \beta_6 + \beta_2 \right]$$

$$= \frac{(\sqrt{n}-1)(-2+n)}{(1+\sqrt{n})^6 n^3} \left(37 + 31\sqrt{n} + 10n + 40n^{3/2} + 29n^2 - 15n^{5/2} \right.$$

$$\left. - 14n^3 + 4n^{7/2} + 5n^4 + n^{9/2} \right).$$

The final type of term contains mixed second indices between the different rotation matrix powers and we consider the thirteenth sum in equation (24) as a representative of this set. The strategy is the same for all such terms and involves performing the inner summation by extracting the terms with $i = n$ and $j = n$ and performing the summations over j and i, then breaking the remaining restricted sum over $i \neq j \leqslant n - 1$ into the difference of an unrestricted sum over all values of $i, j \leqslant n - 1$ and one with $i = j \leqslant n - 1$. We have

$$(n+\sqrt{n})^8 \sum_{i\neq j}^{n} Q_{ki}^3 Q_{\ell i} Q_{kj} Q_{\ell j} Q_{mj}^2$$

$$= (-1+\alpha_3)(-1+\alpha_1) \sum_{j=1}^{n-1} (-1+\beta_1\delta_{kj})(-1+\beta_1\delta_{\ell j})(1+\beta_2\delta_{mj})$$

$$+ (-1+\alpha_1)^2(1+\alpha_2) \sum_{i=1}^{n-1} (-1+\beta_3\delta_{ki})(-1+\beta_3\delta_{\ell i})$$

$$+ \sum_{i=1}^{n-1} (-1+\beta_3\delta_{ki})(-1+\beta_1\delta_{\ell i}) \sum_{j=1}^{n-1} (-1+\beta_1\delta_{kj})(-1+\beta_1\delta_{\ell j})(1+\beta_2\delta_{mj})$$

$$- \sum_{i=1}^{n-1} (-1+\beta_3\delta_{ki})(-1+\beta_3\delta_{\ell i})^2(-1+\beta_1\delta_{ki})(1+\beta_2\delta_{mi})$$

$$= \left[(-1+\alpha_1)(-1+\alpha_3)(n-1-2\beta_1+\beta_2) + (1+\alpha_2)(-1+\alpha_1)^2(n-1-\beta_1-\beta_3) \right.$$

$$\left. + (n-1-\beta_1-\beta_3)(n-1-2\beta_1+\beta_2) - (n-1-3\beta_1+\beta_2-\beta_3+\beta_1\beta_2+\beta_1^2) \right]$$

and putting everything together:

$$\sum_{k,\ell,m}' \sum_{i,j}' Q_{ki}^3 Q_{\ell i} Q_{kj} Q_{\ell j} Q_{mj}^2 = \frac{(1-\sqrt{n})(n-2)(n-3)}{(1+\sqrt{n})^6 n^3} \left(29 + 39\sqrt{n} + 4n - 28n^{3/2} \right.$$

$$\left. - 12n^2 + 12n^{5/2} + 10n^3 + 2n^{7/2} \right).$$

ORCID iDs

Adrian Del Maestro ● https://orcid.org/0000-0001-9483-8258

References

[1] Essam J W 1971 *Discrete Math.* **1** 83
[2] Anderson P W 1958 *Phys. Rev.* **109** 1492
[3] Abou-Chacra R, Thouless D J and Anderson P W 1973 *J. Phys. C: Solid State* **6** 1734
[4] Georges A, Kotliar G, Krauth W and Rozenberg M J 1996 *Rev. Mod. Phys.* **68** 13
[5] Lichtenstein A I and Katsnelson M I 2000 *Phys. Rev.* B **62** R9283
[6] Hastings M 2003 *Phys. Rev. Lett.* **90** 148702
[7] Burioni R, Cassi D and Destri C 2000 *Phys. Rev. Lett.* **85** 1496
[8] Laumann C R, Parameswaran S A and Sondhi S L 2009 *Phys. Rev.* B **80** 144415
[9] Murray J, Del Maestro A and Tešanović Z 2012 *Phys. Rev.* B **85**
[10] Burioni R, Cassi D, Rasetti M, Sodano P and Vezzani A 2001 *J. Phys. B: At. Mol. Opt. Phys.* **34** 4697
[11] Hagberg A A, Schult D A and Swart P J 2008 Exploring network structure, dynamics, and function using networkx *Proc. of the 7th Python in Science Conf.* ed G Varoquaux *et al* p 11
[12] Steger A and Wormald N 1999 *Comb. Probab. Comput.* **8** 377
[13] Kim J H and Vu V H 2003 *Proc. of the 35th ACM Symp. on Theory of Computing*
[14] Hoory S, Linial N and Wigderson A 2006 *Bull. Am. Math. Soc.* **43** 439
[15] Kesten H 1959 *Trans. Am. Math. Soc.* **92** 336
[16] McKay B D 1981 *Linear Algebr. Appl.* **40** 203
[17] Tran L V, Vu V H and Wang K 2013 *Random Struct. Algorithms* **42** 110
[18] Dumitriu I and Pal S 2012 *Ann. Probab.* **40** 2197
[19] Metz F L, Parisi G and Leuzzi L 2014 *Phys. Rev.* E **90** 052109
[20] Bauerschmidt R, Huang J and Yau H T 2016 arXiv:1609.09052
[21] Bauerschmidt R, Knowles A and Yau H T 2017 *Commun. Pure Appl. Math.* **70** 1898
[22] Deift P 2007 Universality for mathematical and physical systems *International Congress of Mathematicians. Vol.* I (Zürich: European Mathematical Society) p 125
[23] Jakobson D, Miller S D, Rivin I and Rudnick Z 1999 Eigenvalue spacings for regular graphs *Emerging Applications of Number Theory* (New York: Springer) pp 317–27
[24] Oren I and Smilansky U 2010 *J. Phys. A: Math. Theor.* **43** 225205
[25] Bauerschmidt R, Huang J, Knowles A and Yau H T 2017 *Ann. Probab.* **45** 3626–63
[26] Friedman J 1993 *Duke Math. J.* **69** 487
[27] Elon Y 2008 *J. Phys. A: Math. Theor.* **41** 435203
[28] Dekel Y, Lee J R, Linial N and Linial N 2010 *Random Struct. Algorithms* **39** 39
[29] Kabashima Y and Takahashi H 2012 *J. Phys. A: Math. Theor.* **45** 325001
[30] Brooks S and Lindenstrauss E 2012 *Isr. J. Math.* **193** 1
[31] Geisinger L 2015 *J. Spectr. Theor.* **5** 783
[32] Bourgade P, Huang J and Yau H T 2017 *Electron. J. Probab.* **22** 64
[33] Backhausz A and Szegedy B 2016 arXiv:1607.04785
[34] Bollobás B 1980 *Eur. J. Comb.* **1** 311
[35] OEIS Foundation Inc. 2018 The on-line encyclopedia of integer sequences (http://oeis.org/A002851)
[36] Füredi Z and Komlós J 1981 *Combinatorica* **1** 233
[37] Bell R J and Dean P 1970 *Discuss. Faraday Soc.* **50** 55
[38] Visscher W M 1972 *J. Non-Cryst. Sol.* **8–10** 477
[39] Cizeau P and Bouchaud J 1994 *Phys. Rev.* E **50** 1810
[40] Cavagna A, Giardina I and Parisi G 1999 *Phys. Rev. Lett.* **83** 108
[41] Metz F L, Neri I and Bollé D 2010 *Phys. Rev.* E **82** 031135
[42] Slanina F 2012 *Eur. Phys. J.* B **85** 1
[43] Cramér H 1999 *Mathematical Methods of Statistics* (*Princeton Landmarks in Mathematics*) (Princeton, NJ: Princeton University Press) (reprint of the 1946 original)
[44] Muller M E 1959 *Commun. ACM* **2** 19–20
[45] Folland G B 2001 *Am. Math. Mon.* **108** 446
[46] Meringer M 1999 *J. Graph Theory* **30** 137